

Nanoscale

Accepted Manuscript



This is an *Accepted Manuscript*, which has been through the Royal Society of Chemistry peer review process and has been accepted for publication.

Accepted Manuscripts are published online shortly after acceptance, before technical editing, formatting and proof reading. Using this free service, authors can make their results available to the community, in citable form, before we publish the edited article. We will replace this *Accepted Manuscript* with the edited and formatted *Advance Article* as soon as it is available.

You can find more information about *Accepted Manuscripts* in the [Information for Authors](#).

Please note that technical editing may introduce minor changes to the text and/or graphics, which may alter content. The journal's standard [Terms & Conditions](#) and the [Ethical guidelines](#) still apply. In no event shall the Royal Society of Chemistry be held responsible for any errors or omissions in this *Accepted Manuscript* or any consequences arising from the use of any information it contains.

Healing defective CVD-graphene through vapor phase treatment

Do Van Lam,^{1,2} Sang-Min Kim,² Youngji Cho,³ Jae-Hyun Kim,² Hak-Joo Lee,² Jun-Mo Yang³
and Seung-Mo Lee^{1,2,*}

¹ Nano Mechatronics, University of Science and Technology (UST), 217 Gajeong-ro, Yuseong-gu, Daejeon 305-333, South Korea

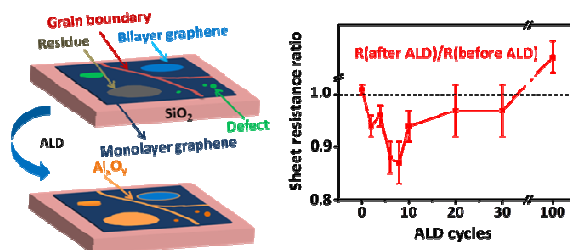
² Department of Nanomechanics, Korea Institute of Machinery and Materials (KIMM), 156 Gajeongbuk-ro, Yuseong-gu, Daejeon 305-343, South Korea

³ Department of Measurement & Analysis, National Nanofab Center, 291 Daehak-ro, Yuseong-gu, Daejeon 305-701, South Korea

* Corresponding authors: ^{1,2} sm.lee@kimm.re.kr

Supporting information included.

TOC Graphic and Summary



“Structural defects present on CVD-graphene, which are originated from growth stage and transfer process, can be selectively healed by vapor phase treatment performed in equipment conventionally used for atomic layer deposition. The treated graphenes show noticeably improved electrical properties with long term stability in contrast with chemically doped graphenes.”

Abstract

Structural defects present on chemical vapor deposition (CVD)-graphene are usually originated from growth stage and transfer process. Those limit the electronic transport properties of the graphene and degrade performance of related devices. Here we report that those inherent atomic defects could be selectively healed by simple vapor phase treatment performed in equipment conventionally used for atomic layer deposition (ALD). The unique chemistry of Al_2O_3 ALD facilitated selective depositions of Al_xO_y compounds on the defects, which was able to be readily probed and visualized using AFM imaging. The healing agent, Al_xO_y , was observed to bind tightly to the defects and lead to doping of the CVD-graphene, which were reflected in noticeable improvement in the electrical sheet resistance. In contrast with the chemically doped graphene, the ALD treated graphenes revealed notable long term stability under environmental conditions. Our approach promises selective healing of defects present in most of materials and likely ensures considerable improvement in electrical and mechanical properties. The ALD with a broad spectrum of material selection could be a versatile tool for upgrading materials' properties.

Keywords: CVD-graphene, Atomic Layer Deposition (ALD), 2-dimensional defects

MAIN TEXT

Defect in 2-D materials, i.e. irregular arrangement of atoms, is a crucial factor to dominate materials properties [1, 2]. A single-atomic thick graphene grown by chemical vapor deposition (CVD) [3-5] unavoidably contains structural defects such as grain boundaries and dislocations. Grain boundaries are originated from joining of grains during initial growth stage. Differences in grain orientation create line defects at interfaces. The transfer process of CVD-graphene grown on Cu foil to another substrate also creates other macroscopic defects such as folds, cracks, wrinkles, and residues. These defects lead to scattering of charge carriers [1, 6], which limits the electronic transport properties of the graphene and thus determines performance of related devices. The transport properties of the graphene have been reported to be improved by enlarging grain sizes [7], producing overlapped grain boundaries by extended growth [8], healing structural defects by high-temperature processing [9], increasing carrier density through chemical doping [10], or bridging graphene grains using metal nanowires [11]. However, these approaches are often limited to stability and/or flexibility to applications. Here, we report that the atomic defects present in the CVD-graphene can be selectively healed by vapor phase treatment performed in equipment conventionally used for atomic layer deposition (ALD). A few cycles of metal oxide ALD on the graphene greatly improved electrical sheet resistance. The unique ALD chemistry enabled the defects to be selectively healed and plainly visualized. We discuss the effect of ALD treatment of the graphene on the structural defects on the basis of results obtained from some characterization tools. Our results suggest new pathways for tailoring properties of the graphenes and other 2-D materials by healing the atomic defects inevitably present on them.

ALD is based on surface chemistry of the substrate material. An inert surface without dangling bonds, like a defect-free pristine graphene, is chemically passive to ALD precursors [12]. In contrast, the CVD-graphene containing lots of the atomic defects can be naturally expected to offer preferential nucleation sites for ALD. In other words, at the initial stage of ALD, deposition occurs selectively and primarily at the defect sites on the CVD-graphene prior to full coverage (Fig. 1a). Consequently, this technique is possibly used to probe and visualize graphene defects. For the preparation of the graphene on SiO₂ substrates, CVD-graphene was prepared by a wet-etching process (Fig. S1). Among lots of available ALD materials, in this study, Al₂O₃ ALD with trimethylaluminum (TMA) and H₂O was selected in consideration of reactivity of the precursor and processibility at low temperature [13]. First, Al₂O₃ was deposited on the raw transferred graphene and surface coverage of Al₂O₃ was observed to be quite dense. Considering the fact that the polymer layer used for transferring the graphene is hard to completely remove by etching [14], Al₂O₃ appeared to be deposited primarily on the polymer residue rather than on the graphene defects (Fig. S2). Hence, prior to ALD, all samples were annealed at 350 °C to prepare clean graphenes with least residues and concurrently stabilized electrical sheet resistances (Table S1). Figure 1b shows a high resolution transmission electron microscopy (HR-TEM) image of a monolayer graphene treated with 4 cycles of Al₂O₃ ALD (precursors: TMA and H₂O) and its corresponding fast Fourier transform (FFT) image. Two distinct regions of immaculate graphene and graphene/adsorbates were observed. The latter was supposed to be defect sites of the CVD-graphene which function as nucleation sites for deposition.

Effects of ALD-based vapor phase treatment on CVD-graphene were firstly examined by comparison of electrical sheet resistance changes (measured by 4-point probe method)

before and after ALD (Fig. 1c). Freshly transferred graphenes without annealing were initially studied. However, negligible reduction in sheet resistance was recorded with various ALD cycles (Fig. S3). It is well known that large amount of polymethylmethacrylate (PMMA) residues remain on the graphene unless the transferred graphenes are annealed. Beyond doubt, those residues offer good nucleation sites for Al_2O_3 deposition. It means that most of the non-annealed graphenes are unnecessarily covered with Al_2O_3 layer, which naturally serves as electrical insulation layer. Therefore, any significant improvement in the sheet resistance was not able to be expected. Contrastively, upon few ALD cycles on the annealed graphenes, there were noticeable reductions in sheet resistance ($\sim 15\%$) for the graphenes treated with 6 and 8 ALD cycles. Experimentally, the measurement using probes always induces some damages to the graphenes depending on the size of probes used and the repeating times of measurements (Fig. S4). Hence, we believe that, in practice, the ALD treated graphenes should have much lower sheet resistances. Nucleation and growth of Al_2O_3 on the graphene during ALD are highly dependent on the reaction of the surface species with gas phase precursors [12]. The surface reactions continue until the initial graphene surface is completely converted to Al_2O_3 surface. As can be noticed from the sharp increase in sheet resistance, it was not until 100 cycles of ALD that Al_2O_3 covers the entire graphene surface. The variations in water contact angles were also indicative of incomplete coverage of Al_2O_3 on the graphene below 100 cycles of ALD (Fig. 1d). While the clean CVD-graphenes without ALD-treatment showed the contact angle of 84.7° , the ALD-treated graphenes showed a noticeable increase (e.g. 10° after 8 ALD cycles). Upon 100 ALD cycles, the contact angle dramatically decreased ($\sim 19^\circ$).

The evolution of the graphene surface with different Al₂O₃ ALD cycles was studied by atomic force microscopy (AFM). Firstly, the topographic image of the bare graphene surface was imaged (Fig. 2a). A large number of wrinkles with an average height of ~ 2 nm were observed on the relatively flat graphene surface. At 10 ALD cycles, wrinkles (1-dimensional line defects) and presumable nucleation sites (likely, 0-dimensional point defects) with heights of ~ 4 nm and ~ 2 nm were clearly visualized, respectively (Fig. 2b). Considering the observation that the ALD materials nucleated and grew with a similar speed on both wrinkles and point defects, the ALD on the CVD-graphene appears to be less limited by the sizes or dimensions of the existing defects. Moreover, the lateral force measurement given by the contact-mode scanning revealed that the ALD treated graphenes have higher friction force than the bare graphenes. It indicated that bonding between the graphene and the Al₂O₃ nuclei is quite tight (Fig. S5). The nuclei grew bigger and began to join adjacent nuclei to form clusters of Al₂O₃. Upon 100 ALD cycles, a patchy and discontinuous film with pinholes was formed (Fig. 2c). The corresponding schematics of the ALD treated graphenes were depicted (Fig. 2d-f). In general, except macroscopic defects such as wrinkles and contaminated particles, other atomic defects of the graphenes were hardly probed using AFM. However, the vapor phase treatment of the graphene by few cycles of ALD enabled the defects to be clearly visualized using AFM (Fig. 2e).

Figure 3a shows a HR-TEM image of the graphene treated with 4 Al₂O₃ ALD cycles. The presence of 2 grains in each separated region (marked with red and blue color, respectively) is identified from the corresponding FFT images (Fig. 3b, c). The FFT image of the whole Fig. 3a indicates the presence of 3 grains. The graphene is likely composed of double layer with 1 basal grain and 2 upper grains. The boundary between those 2 upper grains, on which a

large patch likely having Al elements exist, is denoted by the approximate yellow line. In our experiments, we transferred the graphenes onto TEM grids with both a polymer-supported transfer method and a direct transfer method. The former one was problematic due to the adsorbates. The same situation occurred for the case of the latter. Though the exact source of the adsorbates is unclarified, the graphenes were thought to be contaminated during the transfer process, and the grain boundaries appeared to provide sites for adsorbates to be easily bound. The adsorbates were able to be minimized by annealing over the temperature of 350 °C [15]. Figure 3e is a dark-field TEM image of the graphene sample and its corresponding EDX mapping of Al (Fig. 3f). The presence of Al is on specific areas only, which is similar for ALD of TiO₂ [16] and Pt [17] on graphene nanosheets. It appears that regions with/without Al are defective/pristine areas of the graphene, respectively.

The chemical compositions and binding states of the ALD-treated graphenes were studied by X-ray photoelectron spectroscopy (XPS) (Fig. 3g, h). The presence of Al was detected in the samples, even with only 2 ALD cycles. The C 1s peak located at 284.6 eV was attributed to sp^2 bonding of carbon atoms in graphene [18]. The Al 2p peak at 74 eV was assigned to Al metal, while the peak at 76 eV was originated from Al₂O₃ [19]. The peaks of Al 2p and C 1s were both upshifted after ALD. A lower binding energy is generally associated with oxygen deficiency. Therefore, the upshift indicates an increase in number of Al-O bond with ALD cycles, which could be also related to doping of graphene by ALD reactants, as can be recognized from Raman spectroscopy results (Fig. 4). At the few ALD cycles, the Al 2p peaks are between Al and Al₂O₃ peaks, which imply the existence of the compound Al_xO_y on the graphene. In short, the existence of Al_xO_y could refer to healing of defects on CVD-graphene, thereby leading to the doping and the improved electrical properties.

Raman spectroscopy was employed to confirm doping effect through vapor phase treatment. The spectra show common G and 2D band peaks of the graphenes, which lie at $\sim 1600\text{ cm}^{-1}$ and $\sim 2700\text{ cm}^{-1}$, respectively (Fig. 4a). It is interesting that both G and 2D bands were highly blueshifted from 1598 to 1603 cm^{-1} and 2698 to 2707 cm^{-1} for the graphene treated with 8 ALD cycles, respectively. Since the graphenes were annealed before ALD, the doping effects by water and residues were negligible. Presumable doping by annealing and straining effect could be excluded because the ALD treatment was performed at low temperature of $100\text{ }^{\circ}\text{C}$. Thus, the existence of the Al_xO_y compounds at the graphene defects are thought to be the most probable reason causing the blueshifts in the Raman spectra. For clearer validation, the correlation between position of G and 2D peaks was presented (Fig. 4b). The variation of 2D peak is mainly due to the charge transfer, in which blueshifts/redshifts are referred as hole/electron doping, respectively [20]. The stiffening of 2D peaks with increasing the position of G peaks suggests the p-type doping by few cycles of Al_2O_3 ALD on CVD-graphene. Normally, chemical doping of graphene films are limited in stability, such as a 40% increase in the sheet resistance during a few days [10, 21]. However, the sheet resistances of the ALD treated graphenes were observed to remain nearly unchanged even after one month (Fig. S6). The Al_xO_y compounds on the ALD-treated graphenes likely act as a barrier that prevents the graphenes from oxidation.

In conclusion, we found that the inherent atomic defects existing on the CVD-graphene could be effectively healed through the vapor phase treatment provided by ALD. The unique nucleation/growth mechanism of ALD facilitated selective depositions of Al_xO_y compounds primarily on the defects, which was able to be readily probed and visualized using AFM imaging. The healing agent, Al_xO_y , was observed to bind tightly to the defects and lead to

doping of the CVD-graphene, which were reflected in noticeable improvement in the electrical sheet resistance. More importantly, by contrast to the chemically doped graphene, the ALD treated graphenes revealed notable long term stability under environmental conditions. Our approach promises selective healing of defects present in most of materials and likely ensures considerable improvements in electrical and mechanical properties. In addition, as the ALD tool currently provides a broad spectrum of material selection, it is believed that and ALD could be a versatile tool for upgrading 2D or 3D materials' properties by providing various healing agents for structural defects.

Acknowledgements

This research was supported by the industrial Core Technology Development Programs of the Korean Ministry of Knowledge Economy (grant 10033309), National Platform Technology Programs of the Korean Ministry of Knowledge Economy (grant 10034751), the Center for Nanoscale Mechatronics and Manufacturing, one of the 21st Century Frontier Research Programs of the Korean Ministry of Education, Science and Technology, and Innovative Research Programs of Korean Institute of Machinery and Materials.

Methods

Synthesis of graphene on copper: 25 μm thick Cu foils (Alfa-Aecer; 99.8 %, No. 13382) were inserted into a 2 inch quartz tube, which is loaded inside a horizontal furnace. The tube was pumped to 600 mTorr, then heated up to 1000 $^{\circ}\text{C}$ with 50 sccm Ar and 20 sccm H₂ mixture flow. It took around 50 min for both heating up and annealing. Subsequently, graphene growth was carried out for 30 min under the mixture flow of 30 sccm CH₄ and 20 sccm H₂. In order to induce slow cooling and prevent the tube from cracking, the furnace lid was kept

closed until the temperature reached 800 °C. Then, the sample was rapidly cooled down by opening the lid of the furnace and blowing air.

Graphene transfer onto SiO₂ substrate: The as-synthesized CVD-graphene on Cu foil was cut into square pieces of 2 x 2 cm. Polymethylmethacrylate (PMMA; Microchem, Inc. 950 A4) was used as scarified layer by spin coating on the top of graphene at 2500 rpm in 30 s. The samples were then put onto an 80 °C hot plate for 2 min to harden the PMMA layer. Since graphene was grown on both sides of the samples, one side was etched away by oxygen plasma at chamber pressure 0.3 torr for 10 s. To etch Cu, the PMMA coated samples were placed floating on ammonium persulfate solution ((NH₄)₂S₂O₈, APS, 0.1 M) overnight. The floating PMMA/graphene films were transferred to a flat beaker and rinsed with deionized water for several times. The oxygen plasma treated 300 nm thick SiO₂/Si substrates were used to scoop the films. The samples were naturally dried in air for 2 h and baked on a hot plate of 110 °C for 1 h to enhance the adhesion of graphene with SiO₂ substrate. Subsequently, the samples were submerged into a beaker of warm acetone (60 °C) for 1 h to remove the polymer layer. To minimize the effects of polymer residues, the graphenes transferred on SiO₂ substrates were annealed in 500 sccm Ar flow at 350 °C for 1 h, prior to ALD.

ALD on CVD-graphene: The annealed graphenes were loaded into a thermal ALD chamber (S200, Savannah) of 100 °C and 20 sccm N₂ flow. To minimize effects of H₂O vapor absorbed on the sample surface, the samples were kept in the chamber for 30 min before ALD. The deposition was carried out at 100 °C using trimethylaluminum (Al(CH₃)₃, TMA, Aldrich, 99.99%) and H₂O as precursors. The ALD was set in exposure mode to ensure the uniform deposition of Al₂O₃. For each ALD cycle, water pulse was 0.1 s in duration, followed by a 20 s exposure, and 30 s purging time, respectively; 0.015 s TMA pulse, 20 s exposure, and 30 s purging time, correspondingly. We also put Si pieces as reference samples to estimate growth rate of Al₂O₃.

Electrical sheet resistance: The sheet resistance was measured using the four-point probe system (CM-100, AiT). For studying effects of ALD, the sheet resistance data was taken from the same samples before and after ALD.

Water contact angle: A contact angle measuring system (DSA 100, Krüss®) was used to study change in surface chemistry of the samples after ALD. Droplets of 3 μl water were manually dropped onto the surface of these samples at various locations. The data was collected from at least 6 different locations for each sample.

Scanning electron microscopy (SEM): A scanning electron microscopy (Nova Nanosem 200, FEI) was used to examine the surface morphology of the samples at different accelerating voltages to obtain good contrast at different magnifications.

Atomic force microscopy (AFM): The topographic images were obtained using a XE-100 system (Park systems) in both contact mode and non-contact mode. The force applied to the AFM tip was about 5 nN. The scan rate was 0.5 Hz. The scan size of each image was 5 x 5 μm with resolution of 256 x 256 pixels.

X-ray Photoelectron spectroscopy (XPS): XPS was performed using an Al K α X-ray source (Multilab 2000, Thermo). The spot size for each measurement is 0.5 μm^2 .

Transmission electron microscopy (TEM): The graphene on Cu foil was transferred to an Au Quantifoil® TEM grid using the PMMA based transfer and direct transfer technique. The procedure of the PMMA based transfer technique was the same as transferring graphene on SiO₂ substrates. For achieving clean graphene with least residue, the graphene/TEM grid was further annealed as mentioned above. In case of direct transfer method, the TEM grid was placed in contact with a small piece of graphene/Cu and heated to 100 °C on a hot plate. A droplet of isopropanol (C₃H₈O, IPA; Sigma-Aldrich, 99.7 %) was dropped onto the surface of TEM grid and graphene/Cu. After IPA was completely evaporated, the TEM grid strongly attached to the graphene/Cu sample. Subsequently, the sample was placed floating on APS solution for 2 h. Normally, it took around 5 h to etch Cu completely. The sample was then moved to new APS solution to ensure that unused graphene on the other side of Cu foil was washed away. The graphene/TEM grid was then rinsed in deionized water several times and dried in air. Finally, the grids were put into the ALD reactor with the above recipe for ALD treatment. The TEM images were taken using an HR-TEM instrument (JEM-ARM200F, Jeol) at 80 kV. The TEM energy dispersive X-ray spectroscopy (TEM-EDX) mapping was

implemented to examine the distribution of chemical elements on the surface of the samples.

Raman spectroscopy: A Raman spectroscopy (inVia Raman microscope, Renishaw) was used to study the doping of CVD-graphene by ALD treatment. The Raman spectrometer was equipped with 514 nm laser line and an objective (x100). The backscattered Raman light was diffracted by an 1800 gr/mm grating. To avoid local heating effects, the laser power density was kept below $100 \mu\text{W}/\mu\text{m}^2$.

Notes and references

- 1 O. V. Yazyev and S. G. Louie, *Nat. Mater.*, 2010, **9**, 806-809.
- 2 Q. Yu, L. A. Jauregui, W. Wu, R. Colby, J. Tian, Z. Su, H. Cao, Z. Liu, D. Pandey, D. Wei, T. F. Chung, P. Peng, N. P. Guisinger, E. A. Stach, J. Bao, S. S. Pei and Y. P. Chen, *Nat. Mater.*, 2011, **10**, 443-449.
- 3 X. Li, W. Cai, J. An, S. Kim, J. Nah, D. Yang, R. Piner, A. Velamakanni, I. Jung, E. Tutuc, S. K. Banerjee, L. Colombo and R. S. Ruoff, *Science*, 2009, **324**, 1312-1314.
- 4 S. Bae, H. Kim, Y. Lee, X. Xu, J. S. Park, Y. Zheng, J. Balakrishnan, T. Lei, H. R. Kim, Y. Song, Y. J. Kim, K. S. Kim, B. Özyilmaz, J. H. Ahn, B. H. Hong and S. Iijima, *Nat. Nanotechnol.*, 2010, **5**, 574-578.
- 5 X. Li, C. W. Magnuson, A. Venugopal, J. An, J. W. Suk, B. Han, M. Borysiak, W. Cai, A. Velamakanni, Y. Zhu, L. Fu, E. M. Vogel, E. Voelkl, L. Colombo and R. S. Ruoff, *Nano Lett.*, 2010, **10**, 4328-4334.
- 6 H. S. Song, S. L. Li, H. Miyazaki, S. Sato, K. Hayashi, A. Yamada, N. Yokoyama and K. Tsukagoshi, *Sci. Rep.*, 2012, **2**, 337.
- 7 P. M. Ajayan and B. I. Yakobson, *Nat. Mater.*, 2011, **10**, 415-417.

- 8 A. W. Tsen, L. Brown, M. P. Levendoff, F. Ghahari, P. Y. Huang, R. W. Havener, C. S. Ruiz-Vargas, D. A. Muller, P. Kim and J. Park, *Science*, 2012, **336**, 1143-1146.
- 9 I. N. Kholmanov, J. Edgeworth, E. Cavaliere, L. Gavioli, C. Magnuson and S. R. Ruoff, *Adv. Mater.*, 2011, **23**, 1675-1678.
- 10 G. X. Ni, Y. Zheng, S. Bae, C. Y. Tan, O. Kahya, J. Wu, B. H. Hong, K. Yao and B. Özyilmaz, *ACS Nano*, 2012, **6**, 3935-3942.
- 11 I. N. Kholmanov, C. K. Magnuson, A. E. Aliev, H. Li, B. Zhang, J. W. Suk, L. L. Zhang, E. Peng, S. H. Mousavi, A. B. Khanikaev, R. Piner, G. Shvets and R. S. Ruoff, *Nano Lett.*, 2012, **12**, 5679-5683.
- 12 X. Wang, S. M. Tabakman and H. Dai, *J. Am. Chem. Soc.*, 2008, **130**, 8152-8153.
- 13 M. D. Groner, F. H. Fabreguette, J. W. Elam and S. M. George, *Chem. Mater.*, 2004, **16**, 639-645.
- 14 Y. C. Lin, C. Jin, J. C. Lee, S. F. Jen, K. Suenaga and P. W. Chiu, *ACS Nano*, 2011, **5**, 2362-2368.
- 15 Z. Cheng, Q. Zhou, C. Wang, Q. Li, C. Wang and Y. Fang, *Nano Lett.*, 2011, **11**, 767-771.
- 16 X. Sun, M. Xie, G. Wang, H. Sun, A. S. Cavanagh, J. J. Travis, S. M. George and J. Lian, *J. Electrochem. Soc.*, 2012, **159**, 364-369.
- 17 S. Sun, G. Zhang, N. Gauquelin, N. Chen, J. Zhou, S. Yang, W. Chen, X. Meng, D. Geng, M. N. Banis, R. Li, S. Ye, S. Knights, G. A. Botton, T. K. Sham and X. Sun, *Sci. Rep.*, 2013, **3**, 1775.
- 18 A. Felten, A. Eckmann, J. J. Pireaux, R. Krupke and C. Casiraghi, *Nanotechnology*, 2013, **24**, 355705.
- 19 B. R. Strohmeier, *Surf. Interf. Anal.*, 1990, **15**, 51-56.

- 20 C. Casiraghi, S. Pisana, K. S. Novoselov, A. K. Geim and A. C. Ferrari, *Appl. Phys. Lett.*, 2007, **91**, 233108.
- 21 C. Yan, K. S. Kim, S. K. Lee, S. H. Bae, B. H. Hong, J. H. Kim, H. J. Lee and J. H. Ahn, *ACS Nano*, 2012, **6**, 2096–2103.

FIGURES AND CAPTIONS

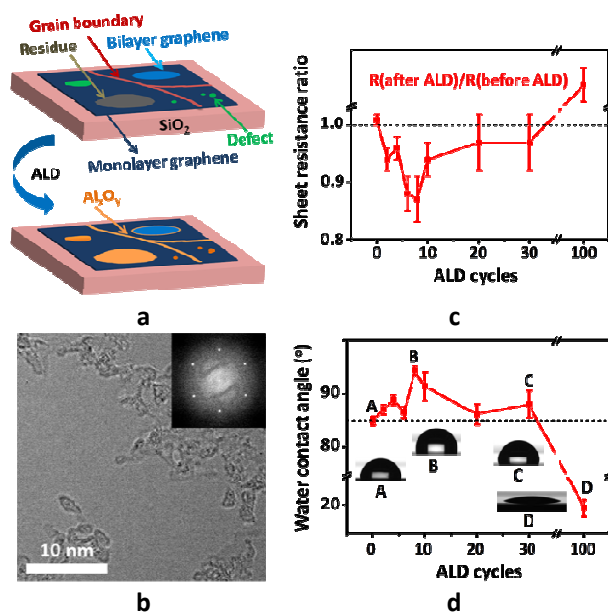


Figure 1. ALD-based vapor phase treatment on CVD-graphene and its resulting healing effects. **a**, Diagram depicting the anticipated effects by ALD treatment on CVD-graphene. By Al₂O₃ ALD, Al₂O₃ or Al_xO_y would be selectively deposited on the specific defect sites on the CVD-graphene. **b**, HR-TEM image of the CVD-graphene after 4 cycles of Al₂O₃ ALD and its corresponding FFT image. **c**, Electrical sheet resistance ratio of the graphene before and after ALD treatment. **d**, Variations in water contact angles with respect to ALD cycles.

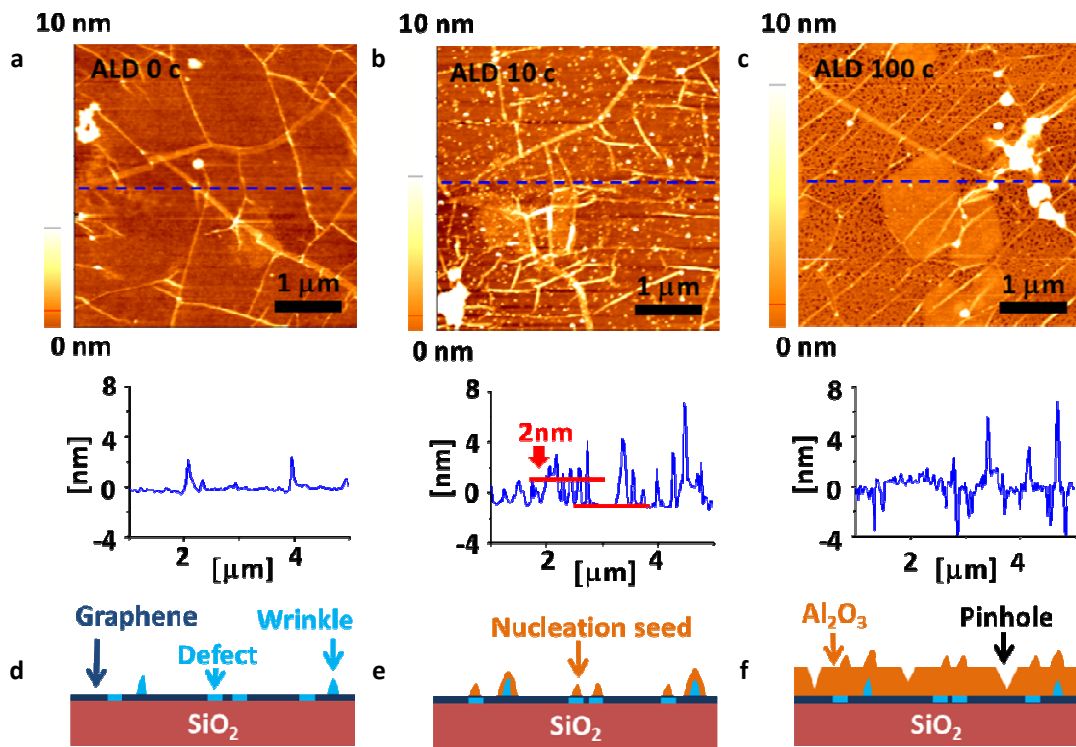


Figure 2. Topographic changes of the CVD-graphene after ALD treatment. **a-c**, AFM images and height profiles of the graphenes after 0, 10, and 100 cycles of Al₂O₃ ALD, respectively. **d-f**, The corresponding schematics of the graphenes on SiO₂ after 0, 10, and 100 cycles of ALD, respectively.

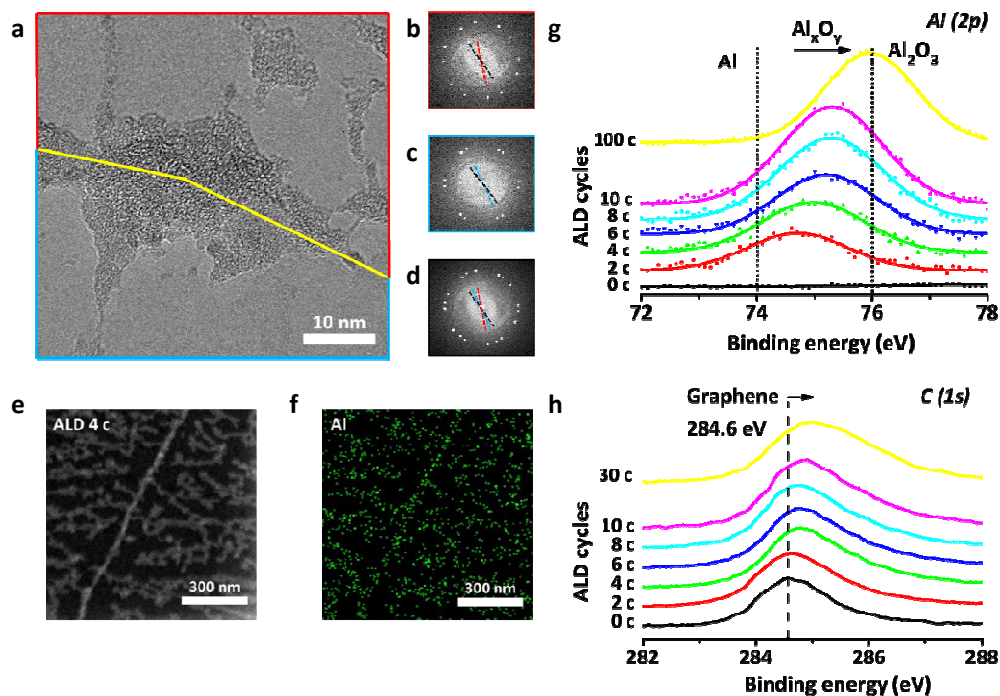


Figure 3. Detection of the grain boundary of the CVD-graphene and elemental analysis of the ALD treated graphene. **a**, HR-TEM image of the graphene treated with 4 cycles of Al_2O_3 ALD. The yellow line denotes approximate line at which the grain boundaries exist (See the text for details). **b**, **c**, FFT image from the upper and lower part of the yellow line in panel **a**, respectively. **d**, FFT image from the whole image in panel **a**. **e**, Dark field TEM image of the graphene treated with 4 cycles of ALD. **f**, The corresponding TEM-EDX elemental mapping of Al in panel **e**. **g**, **h**, XPS spectra of Al $2p$ and C $1s$ with respect to ALD cycles, respectively.

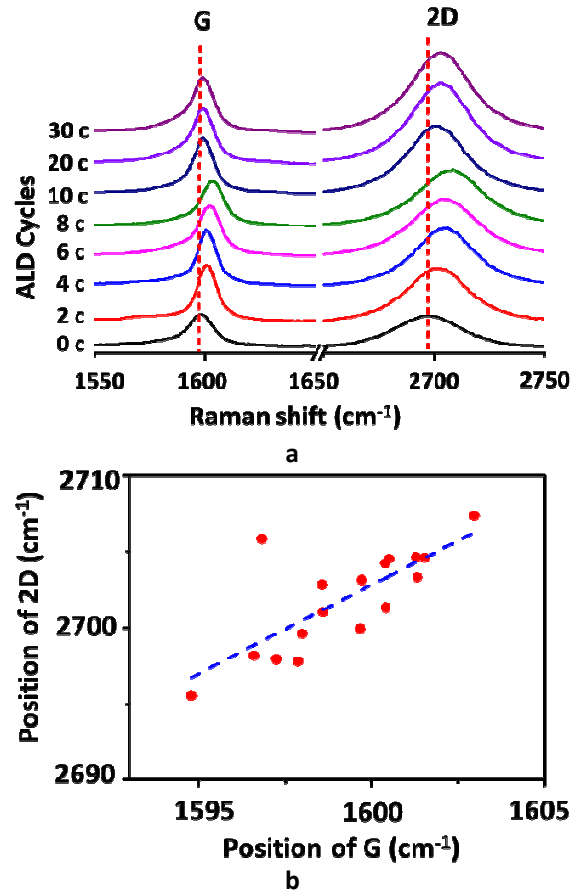


Figure 4. Raman spectra of the graphenes treated with different ALD cycles. **a**, Raman spectra of the graphenes with respect to the number of ALD cycles. **b**, The correlation between peak positions of 2D and G bands.